Materials Science

http://www.aimspress.com/journal/Materials/

AIMS Materials Science, 3(4): 1759-1772.
DOI: 10.3934/matersci.2016.4.1759
Received: 02 October 2016
Accepted: 05 December 2016
Published: 09 December 2016

Research article

A kinematic measurement for ductile and brittle failure of materials using digital image correlation

M.M. Reza Mousavi [1], Masoud D. Champiri [1,*], Mohammad S. Joshaghani [1], and Shahin Sajjadi [2]

[1] Department of Civil and Environmental Engineering, University of Houston, Houston, TX, USA

[2] Department of Construction Management, University of Houston, Houston, TX, USA

[*] **Correspondence:** Email: mdehghanichampiri@uh.edu; Tel: +1-832-620-5366; Fax: +1-713-743-4260.

Abstract: This paper addresses some material level test which is done on quasi-brittle and ductile materials in the laboratory. The displacement control experimental program is composed of mortar cylinders under uniaxial compression shows quasi-brittle behavior and seemingly round-section aluminum specimens under uniaxial tension represents ductile behavior. Digital Image Correlation gives full field measurement of deformation in both aluminum and mortar specimens. Likewise, calculating the relative displacement of two points located on top and bottom of virtual LVDT, which is virtually placed on the surface of the specimen, gives us the classical measure of strain. However, the deformation distribution is not uniform all over the domain of specimens mainly due to imperfect nature of experiments and measurement devices. Displacement jumps in the fracture zone of mortar specimens and strain localization in the necking area for the aluminum specimen, which are reflecting different deformation values and deformation gradients, is compared to the other regions. Since the results are inherently scattered, it is usually non-trivial to smear out the stress of material as a function of a single strain value. To overcome this uncertainty, statistical analysis could bring a meaningful way to closely look at scattered results. A large number of virtual LVDTs are placed on the surface of specimens in order to collect statistical parameters of deformation and strain. Values of mean strain, standard deviation and coefficient of variations for each material are calculated and correlated with the failure type of the corresponding material (either brittle or ductile). The main limiters for standard deviation and coefficient of variations for brittle and ductile failure, in pre-peak and post-peak behavior are established and presented in this paper. These limiters help us determine whether failure is brittle or ductile without determining of stress level in the material.

Keywords: digital image correlation; mortar; aluminum; ductile failure; quasi-brittle failure; statistics

1. Introduction

Brittle and ductile materials are largely used in different branches, e.g., structural engineering. Among brittle materials, concrete-like materials such as mortar are considered challenging since it is non-homogeneous and shows elastic behavior only in a certain range of loading or displacement, but when it reached the plastic region, it initially shows hardening behavior until the compressive strength, then it softens and strength of material is reduced significantly. It is noteworthy that mortar shows plasticity and damage conjointly during this process.

On the other hand, ductile materials like steel and aluminum display simpler behavior compared to concrete materials, whereby softening is not captured during loading scenarios. Aluminum is a homogeneous material with a hardening observed when it reaches the post-peak under tension loading. It is noteworthy that these ductile materials have the same behavior under tension and compression.

Several methods are used for instrumentation of experiments and measure the deformation history of the materials during the test. LVDT or strain gauge based systems provides the so-called smeared strain values between contact points of the sensor, which is not adequate to represent the non-homogeneity of the materials. Non-contact measurement systems are developed to characterize the material behavior in a more detailed fashion. A non-contact digital image correlation system was used in this study.

Digital image correlation (DIC) is extensively used with the ability to capture loads and displacements under different loading states. Willam et al. [1] used DIC system for capturing failure for unreinforced masonry under compression. Beizaee et al. [2] used DIC for error analysis of brittle and ductile materials. Yang et al. [3] used DIC method for proposing a stress-strain relationship of RC elements strengthened with FRP sheets under uniaxial tensile stress. Zomorodian et al. [4] also used this set up to capture crack behavior and crack width of RC elements strengthened with FRP sheets under uniaxial tensile stress. DIC system can be implemeted to measure the strain at high temperature [5, 6]. Another interesting aspect of this DIC systems is its application to build expert systems and evaluation systems in order to distinguish the cause of distress using different branches of artificial intelligence (AI) [7, 8, 9]. Joshaghani et al. [10] developed a new DIC technique and resorted to an algorithm called Remote Gridding System to capture surface strain field of highly plastic materials such as soft soil under large displacements.

In experimental setups, linear variable differential transducers (LVDTs) are largely used to monitor displacements, from small-scale tests to full-scale tests [11]. In DIC systems, users are able to define some virtual LVDTs in different positions and measure the displacement in different directions. These LVDTs don't show a uniform platform near plastic zone. For this reason, some statistical approaches are presented in this paper to better interpret the DIC results and make them more reliable. Model selection deals with the trade-off between the goodness of fit and the complexity of the model [12, 13, 14]. The outline of the paper is as follows: The experimental program is introduced in section 2, then the results of DIC system are presented in section 3. Statistical calculations are shown in section 4. Finally, this paper concludes with remarks.

2. Experimental Program

An experimental program was developed to capture the behavior of ductile and quasi-brittle materials. Two different materials were tested in the laboratory. In order to represent the ductile

failure, aluminum specimen were used under monotonic uniaxial tension. The specimen was machined from two inches diameter round bars. Two ends of the specimen keep it fixed in test frame grips and since they are wider than the central part of the specimen, no failure happens in the grip area. The geometry of aluminum specimen is designed according to the capacity of the test frame and shown in Figure 1. The composition of used 6061-T6 alloy is presented in Table 1.

Table 1. Composition of 6061-T6 alloy.

Al	Mg	Si	Fe	Cu
95.9∼98.6%	0.8∼1.2%	0.4∼0.8%	0∼0.7%	0.15∼0.4%
Cr	Zn	Mn	Ti	other
0.04∼0.35%	0∼0.25%	0∼0.15%	0∼0.15%	0∼0.15%

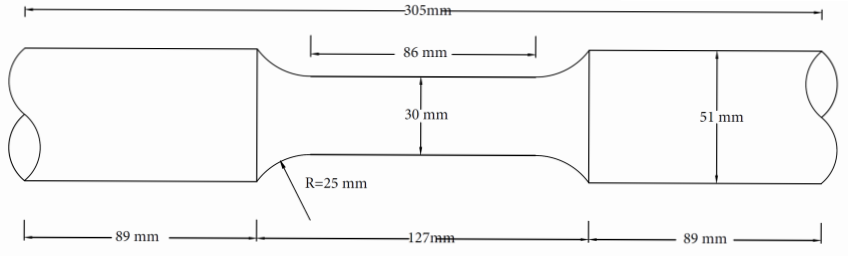

Figure 1. Geometry of tested aluminum specimens.

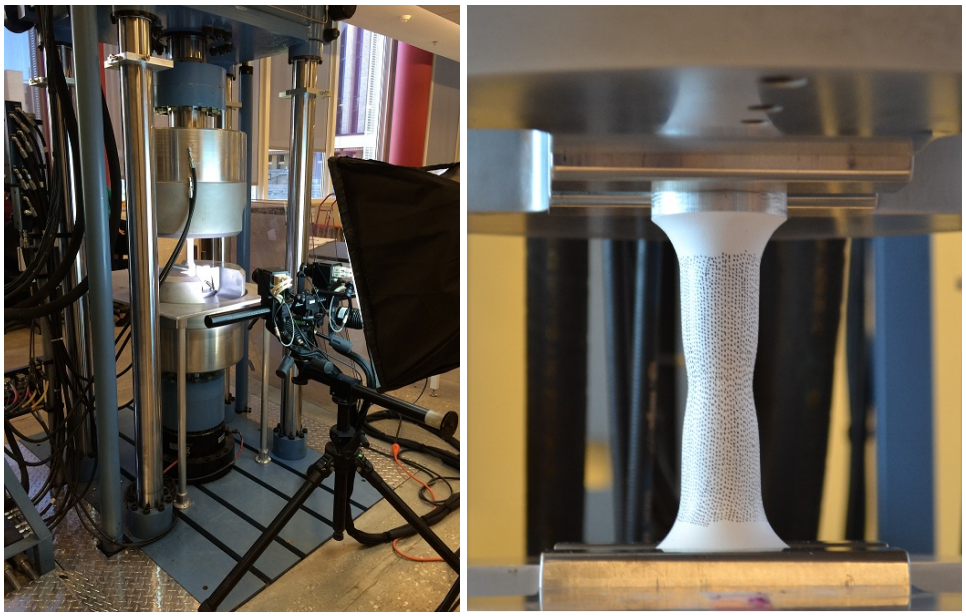

Figure 2. Test frame and specimen setup showing necking behavior.

The experiment was done in a 1200 kN Shorewestern hydraulic axial-torsion testing frame, under displacement control. It is equipped with a 4-column symmetrical construction with a fixed platen and

movable cross head on hydraulic lifts. The test frame and specimen is shown in Figure 2. A rate of 0.635 mm/min was applied to the aluminum specimen.

In order to represent the quasi-brittle failure of mortar, a concrete cylinder which has a radius of 101.6 mm and a height of 203 mm was tested under displacement control uniaxial compression loading with a displacement rate of 0.6 mm/sec approximately equivalent of $\dot{\varepsilon} = 3 \times 10^{-6}/sec$ to represent quasi-static loading (Figure 3).

Figure 3. Mortar specimen inside Tinus Olsen test frame.

Digital Image Correlation (DIC) system was used with ARAMIS software as an optical method for tracking images to accurate 2D and 3D measurements of changes in images. The method determines the displacement history of interest area discretized by facets. DIC tracks the spatial position of the dot pattern painted on the surface of the specimen with respect to so-called start points to determine the deformation field at each stage. The system consisted of two 12 Megapixel digital cameras, to provide a 3D view of specimen, light sources to adjust the amount of light specimen is exposed to, calibration panel to adjust the 3D view of camera and synchronize them with each other, a workstation and software to post process the results and analyze the facet data. The utilized DIC system is shown in Figure 4.

DIC Images were taken at 10-second intervals for aluminum specimens, and this trend remained constant during the testing procedure. This interval was reduced to five seconds for mortar specimens to account for the quasi-brittle nature of the materials. It should be mentioned that in the case of dynamic loading, the intervals between images should be decreased which requires more lighting and storage in the DIC system. For the current experiment, this interval has enough data required for loading steps. The images were then post-processed by DIC software ARAMIS. Strains were computed using directly measured deformation values. Looking at the domain of specimen and distribution of deformation and strain, DIC helps us characterize strong discontinuities which is defined as jumps in the deformation field and/or weak discontinuities in terms of jumps in strain field.

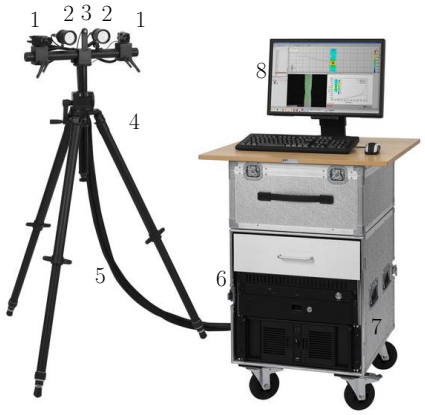

Used DIC system:
1- 12 Megapixel camera
2- Light source
3- Laser pointer
4- Tripod
5- Connection cabe
6- Sensor box
7- Workstation box
8- Software

Figure 4. ARAMIS setup for Digital Image Correlation (DIC).

3. DIC Results

Displacement of each facet is determined using the relative movement of that facet with respect to an assigned starting point. The relative displacement of two facets was then computed relatively, to determine the deformation of the specimen.

The deformation history of an imaginary "virtual LVDT" was computed by monitoring the relative movement of two end facets of the corresponding vLVDT during loading. The reason for using vLVDT (in addition to monitoring the full field deformation) is to provide a representative smeared strain of specimen for determining the stress-strain behavior of the material under applied load history. In the contact point-to-point measurement method, the measured values of deformations are sometimes subjective to the location of the measurement device. In order to reduce this subjectivity, there is a need for installing several measurement devices in different locations, which might not always be feasible. To address this difficulty, numerous vLVDTs were defined on the surface of the specimen to guarantee that the value of smeared strain is a valid representative for the whole specimen.

As shown in Figure 5, the illustrated history consists of 9 vLVDTs defined parallel to the loading axis of the specimen. The smeared stress-strain diagram for this specimen is shown in Figure 6.

The DIC deformation is computed from all 9 vLVDTs for aluminum specimens. The corresponding strain for each vLVDT was calculated based on deformation values of each vLVDT. There are some precise methods to calculate strain values from deformation field captured by DIC [2], but in the present paper, the logarithmic strain was simply calculated using classic method:

$$\varepsilon_T^{vLVDT_i} = Ln\Big(1 + \frac{L_T^{vLVDT_i} - L_0^{vLVDT_i}}{L_0^{vLVDT_i}}\Big) \tag{1}$$

in which, $L_0^{vLVDT_i}$ is the initial length of i^{th} vLVDT, $L_T^{vLVDT_i}$ is the length of i^{th} vLVDT at time T. The obtained strain histories are illustrated in Figure 7.

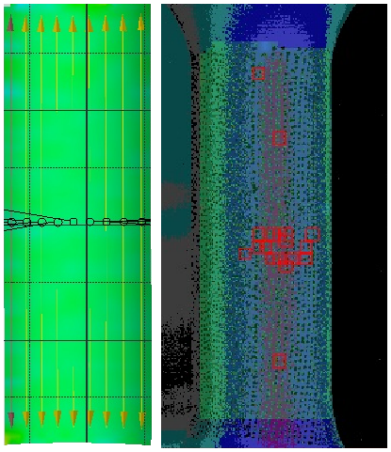

Figure 5. **Arrangement of vLVDTs in aluminum.**

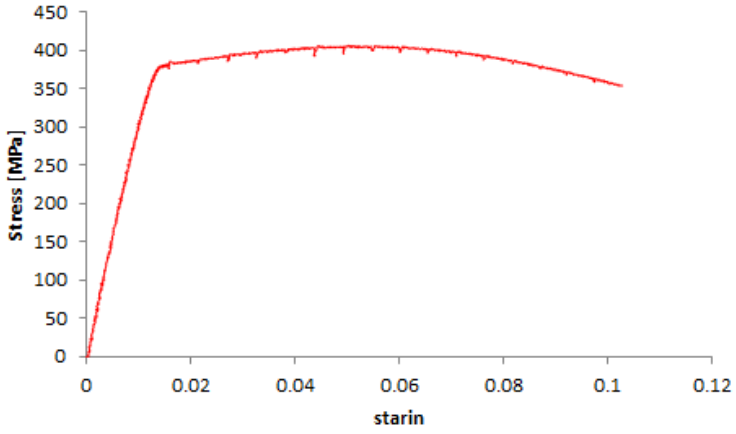

Figure 6. Stress-strain diagram, AL specimen.

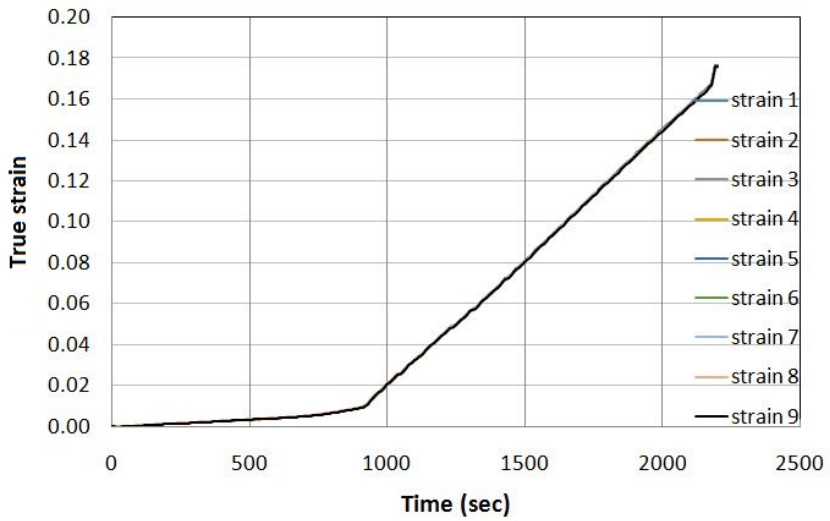

Figure 7. Strain history for aluminum specimens.

An advantage of full field measurement to the point-wise measurement method is that while using full field measurement, we are able to capture all characteristics of deformation field, e.g., strain localization areas and all strain components of any points in critical regions. To better illustrate this, strain localization characterizations and necking of the aluminum specimen have been shown in sequence in Figure 8.

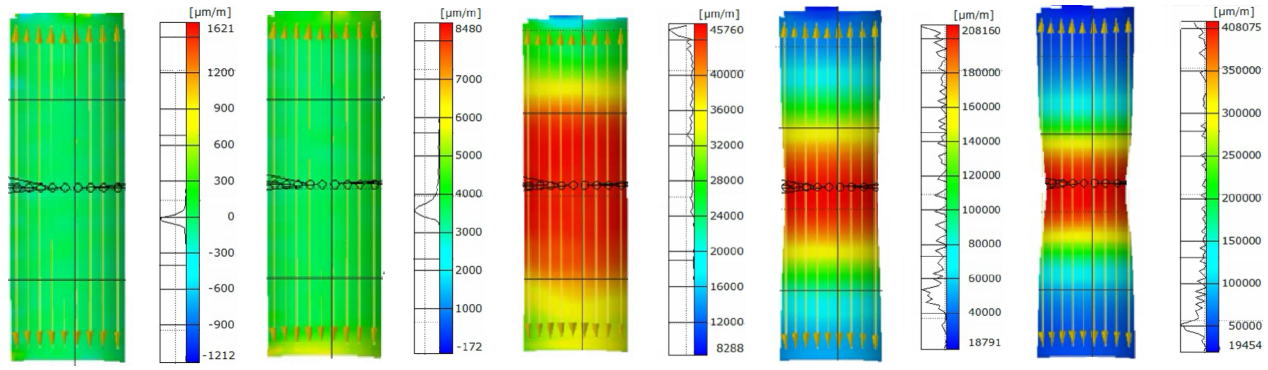

(a) stege 1 **(b) stage 60** **(c) stage 120** **(d) stage 180** **(e) stage 216**

Figure 8. Strain localization for aluminum.

Stress-strain diagram for mortar specimen is shown in Figure 9. The quasi-static nature of mortar can be observed from this diagram. The color pattern and position of vLVDT for mortar specimens are shown in Figure 10. The specimen geometry is discretized into so-called overlapping facets to determine the deformation of the specimen during the testing. The facet size of 12 pixels with overlapping of 25 percent between facets gives us a fine grid of 80 by 200 on the surface of the specimen. The same configuration has been used for the aluminum specimen. It has been demonstrated that the DIC results for the quasi-brittle materials are more scattered than the materials which are ductile. Thus, the number of vLVDTs were more than that of the aluminum specimens. The number of vLVDTs for mortar specimens is 25.

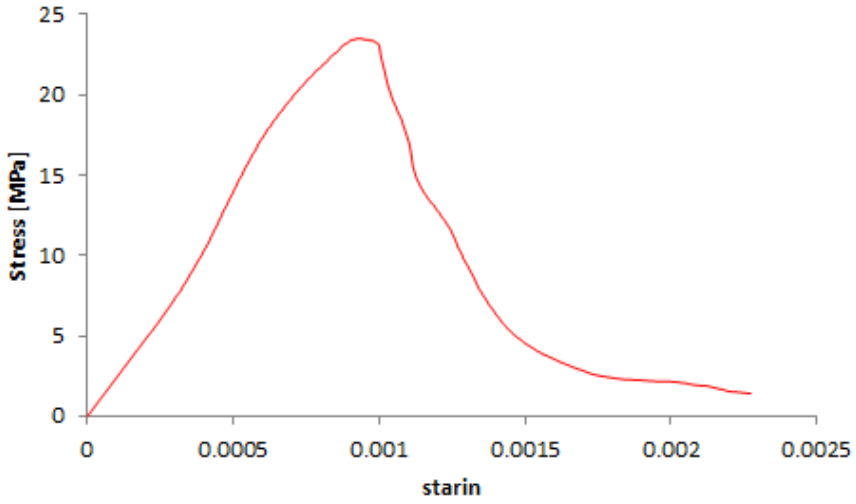

Figure 9. Stress-strain diagram of mortar.

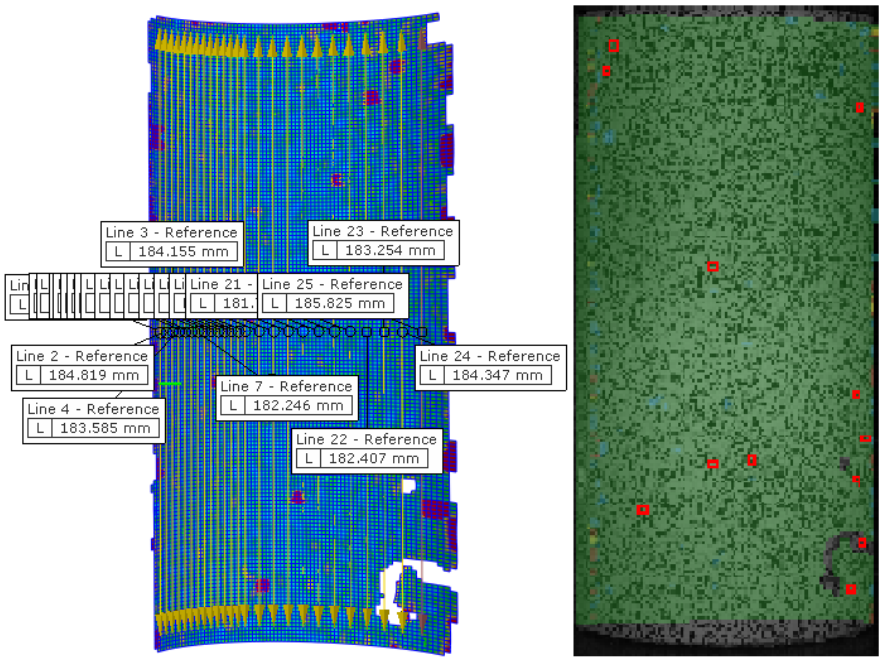

Figure 10. Arrangement of vLVDTs in mortar.

As it can be observed from Figure 11, the history of strain in different regions of the domain has a scatter nature. Since the length of vLVDTs are almost the same, the history of the strains is similar to the history of deformation.

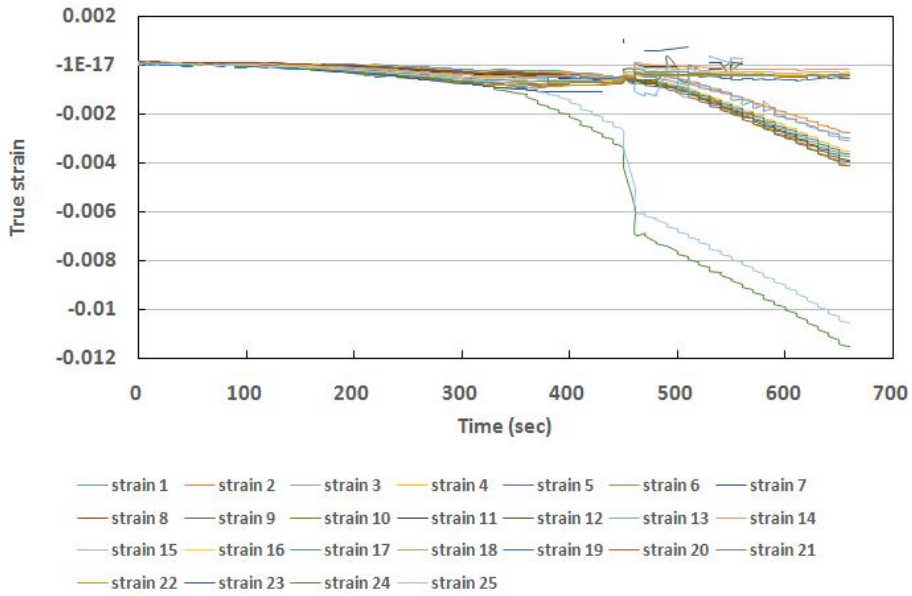

Figure 11. Strain localization for mortar.

During the loading process, the full field representation of strains shows the localization bands and displacement discontinuities in the domain. The crack propagation can be traced from different stages in Figures 12 and 13 along with the axial strain and major strain. The white areas are because of the

imperfections and small holes of the mortar surface which happens sometimes during casting.

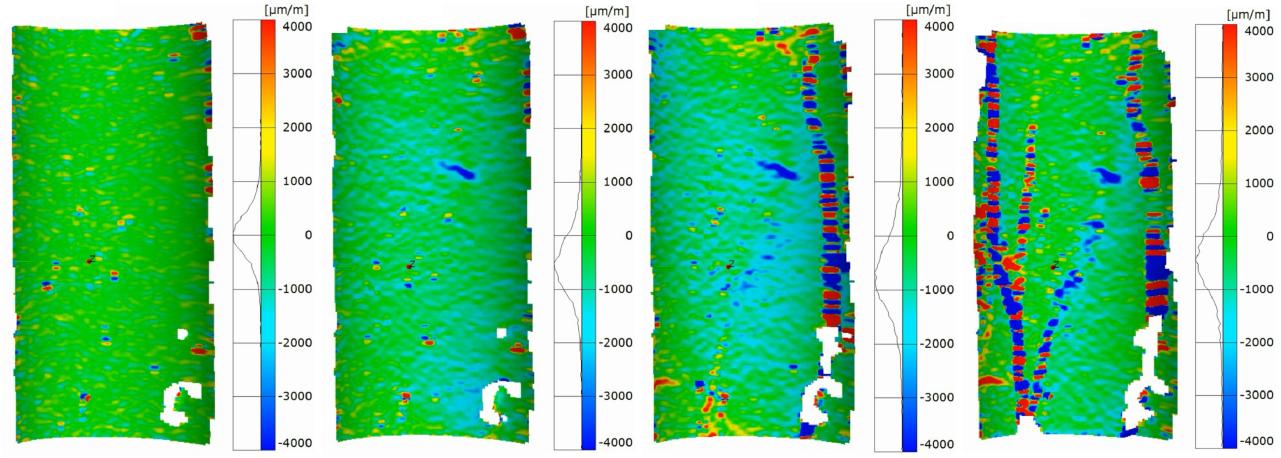

(a) stege 1 **(b) stage 60** **(c) stage 90** **(d) stage 120**

Figure 12. Evolution of axial strain in mortar specimen.

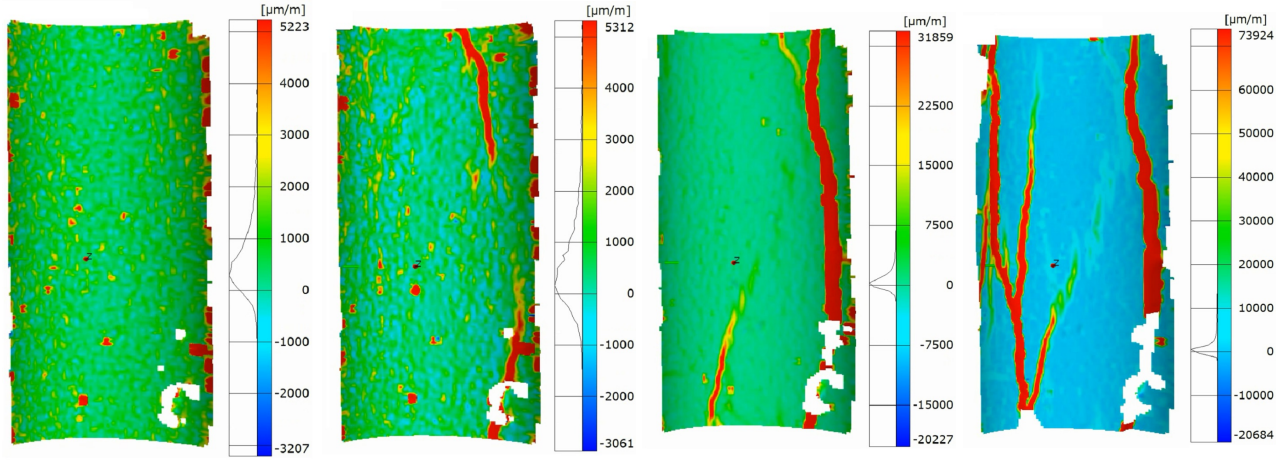

(a) stege 1 **(b) stage 60** **(c) stage 90** **(d) stage 120**

Figure 13. Evolution of major strain and dilation regime in mortar specimen.

4. Statistical Analysis

Hardening in the aluminum specimen started right after yielding of the specimen and the value of plastic strain at the onset of failure is larger than the elastic strain corresponding to yielding stress as shown in Figure 6. As a macroscopic measure of ductility, we can say that $\mu = \frac{\varepsilon_u - \varepsilon_y}{\varepsilon_y} \gg 1$, which is in agreement with the statistical analysis done on DIC results.

Averaging helps us determine a single value of strain at a time vs the stress level to describe material behavior during loading. Using the mean value of elements cannot represent the behavior of system correctly in the engineering point of view. In other words, there is a need to see how data are scattered and spread from the mean value. One of the important indexes is the standard deviation. Standard deviation is a measure of spread, a criterion to check how the data spread over the domain.

A low standard deviation tells us that data are closely observed around the mean or average. A high standard deviation indicates that the data is dispersed over a wider range of values. Standard deviation is used when the distribution of data is approximately resembling the bell curve. Standard deviation is commonly used to understand whether if the specific data are standard and expected or unusual and unexpected.

The average of strain values for both materials is shown in Figure 14 and Figure 15.

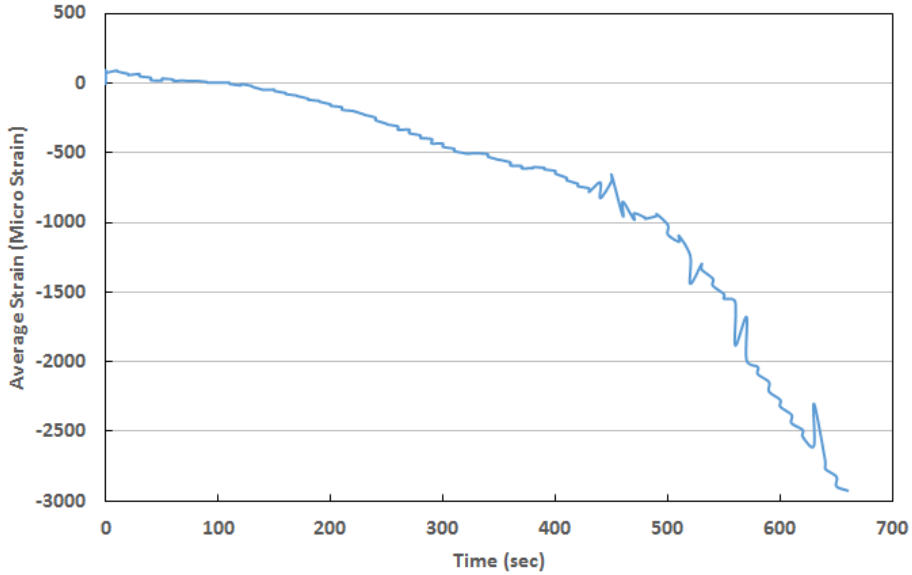

Figure 14. Average strain for mortar.

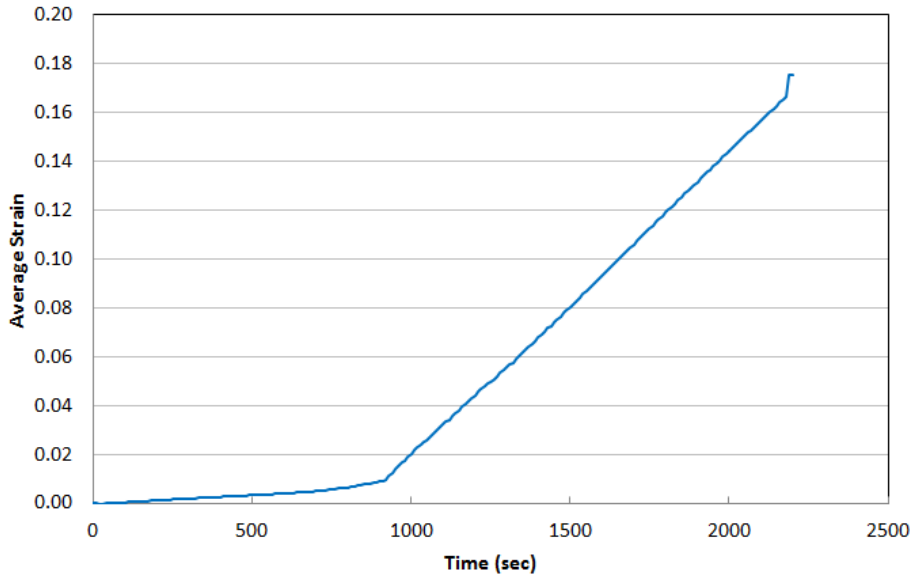

Figure 15. Average strain for aluminum.

Standard variation of mortar specimen is shown in Figure 16; and Figure 17 shows the standard

deviation for the aluminum specimen.

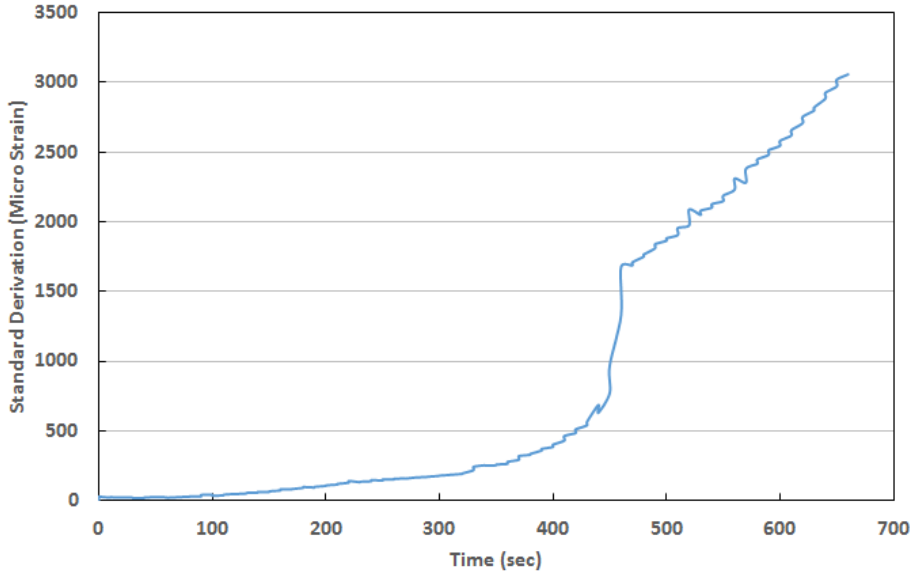

Figure 16. Standard deviation of strain for mortar.

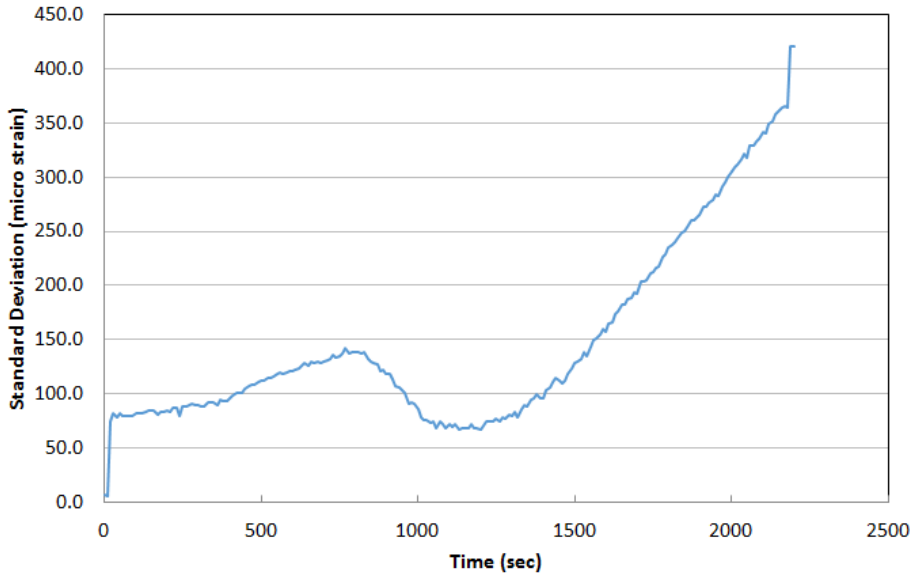

Figure 17. Standard deviation of strain for aluminum.

The coefficient of variation (C_v) is defined as the ratio of the standard deviation (σ) to the mean (μ):

$$C_v = \frac{\sigma}{\mu} \times 100 \tag{2}$$

The coefficient of variation shows the extent of variability in relation to the mean of the population. It allows for meaningful comparisons between two or more magnitudes of variation, even if they have

different means or different scales of measurement. Figure 18 shows the coefficient of variation of the mortar specimen, and coefficient of variation of the aluminum specimen is shown in Figure 19.

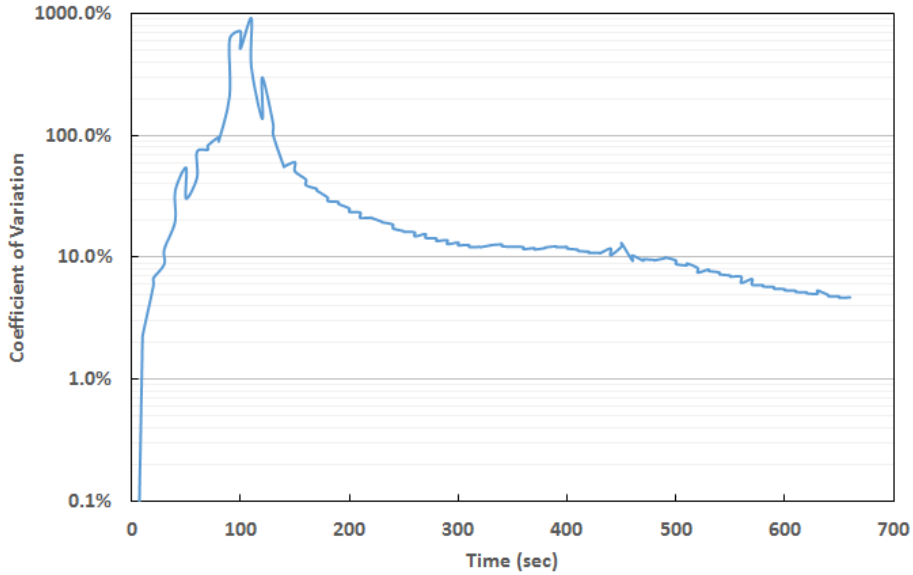

Figure 18. Coefficient of variations of strain for mortar.

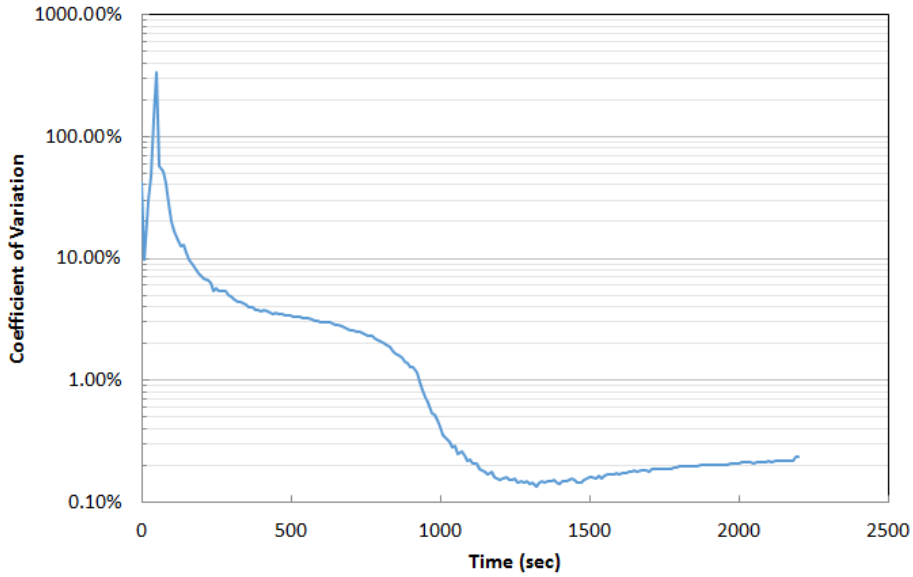

Figure 19. Coefficient of variations of strain for aluminum.

With comparing these statistical results, it is clear that mortar strains are more spread than aluminum and mortar strain is ranged before the peak. When these two materials reach the maximum strength, the data are scattering. During the peak strength, the coefficient of variation of mortar is about 10 times more than the coefficient of variation of aluminum, and coefficient of variation of mortar reaches about

1000% ,which means the strain data are not realistic while this value is about 100% for aluminum. After the peak, this uncertainty decreases rapidly and for mortar is about 10%, while for aluminum is held less than 1% (which is almost negligible). This remarks present that although DIC strain measurement can be preferable during all stages of loading for the aluminum specimen, it cannot be represented correctly during the peak strength of mortar when the material starts softening. So there is a need to remeasure this strain using another approach to avoid the aforementioned uncertainty.

5. Conclusion

Using DIC system, we are able to capture the brittle localized failure and ductile failure in both failure modes. By increasing the strain value, the amount of standard deviation is increased but it doesn't lead to more scattered results. In order to smear out the behavior of brittle materials in terms of a single strain, as representative of whole material behavior, we need to filter out some data points with higher standard deviations from the results in addition to use larger number of vLVDTs.

Different stages of the experiment compared and the strain distributions calculated to come up with appropriate methodologies to detect nature of localized failures on the specimens in terms of ductility or brittleness. The advantage of this method is that we do not need the stress level to determine failure type.

Conflict of Interest

All authors declare no conflict of interest in this paper.

References

1. Willam K, Mohammadipour A, Mousavi R, et al. (2013) Failure of unreinforced masonry under compression. Proceedings of the Structures Congress 2949–2961.
2. Beizaee S, Willam K, Xotta G, et al. (2016) Error analysis of displacement gradients via finite element approximation of Digital Image Correlation system. 9thInternational Conference on Fracture Mechanics of Concrete and Concrete Structures, FraMCoS-9.
3. Yang G, Zomorodian M, Belarbi A, et al. (2015) Uniaxial Tensile Stress-Strain Relationships of RC Elements Strengthened with FRP Sheets. *J Compos Constr* 20: 04015075.
4. Zomorodian M, Yang G, Belarbi A, et al. (2016) Cracking behavior and crack width predictions of FRP strengthened RC members under tension. *Eng Struct* 125: 313–324.
5. Zhou M, Yao WB, Yang XS, et al. (2014) In-situ and real-time tests on the damage evolution and fracture of thermal barrier coatings under tension: A coupled acoustic emission and digital image correlation method. *Surf Coat Tech* 240: 40–47.
6. Wu DJ, Mao WG, Zhou YC, et al. (2011) Digital image correlation approach to cracking and decohesion in a brittle coating/ductile substrate system. *Appl Surf Sci* 257: 6040–6043.
7. Champiri MD, Mousavizadegan SH, Moodi F (2012) A decision support system for diagnosis of distress cause and repair in marine concrete structures. *Comput Concrete* 9: 99–118.

8. Champiri MD, Mousavizadegan SH, Moodi F (2012) A fuzzy classification system for evaluating the health condition of marine concrete structures. *J Adv Concr Tech* 10: 95–109.
9. Champiri MD, Sajjadi S, Mousavizadegan SH, et al. (2016) Assessing Distress Cause and Estimating Evaluation Index for Marine Concrete Structures. *Am J Civ Eng Archit* 4: 142–152.
10. Joshaghani MS, Raheem AM, Mousavi R (2016) Analytical Modeling of Large-Scale Testing of Axial Pipe-Soil Interaction in Ultra-Soft Soil. *Am J Civ Eng Archit* 4: 98–105.
11. Vipulanandan C, Yanhouide JA, Joshaghani SM (2013) Deepwater Axial and Lateral Sliding Pipe-Soil Interaction Model Study. Pipelines 2013: Pipelines and Trenchless Construction and Renewals—A Global Perspective 1583–1592.
12. Gandomi AH, Sajedi S, Kiani B, et al. (2016) Genetic programming for experimental big data mining: A case study on concrete creep formulation. *Automat Constr* 70: 89–97.
13. Kiani B, Gandomi AH, Sajedi S, et al. (2016) New Formulation of Compressive Strength of Preformed-Foam Cellular Concrete: An Evolutionary Approach. *J Mater Civ Eng* 04016092.
14. Sajedi S, Gandomi AH, Kiani B, et al. (2016) Reliability-based multi-objective design optimization of reinforced concrete bridges considering corrosion affect. *ASCE-ASME J Risk Uncertainty Eng Syst Part A: Civ Eng* 04016015.

AIMS Press